Dalton Transactions

ROYAL SOCIETY OF CHEMISTRY

PAPER

View Article Online
View Journal | View Issue

Check for updates

Cite this: *Dalton Trans.*, 2024, **53**, 17841

Fluorescent molecular systems based on carborane-perylenediimide conjugates†

Ruben Rodriguez-Madrid, ‡[a,b] Sohini Sinha, ‡[a] Laura Parejo,[b] Jordi Hernando *[b] and Rosario Núñez *[a]

Received 30th August 2024,
Accepted 9th October 2024

DOI: 10.1039/d4dt02477j

rsc.li/dalton

This study presents the successful synthesis of two perylenediimide (PDI)-based *ortho*-carborane (*o*-carborane) derivatives, **PDI–CB1** and **PDI–CB2**, through the insertion of decaborane into alkyne-terminated PDIs (**PDI1** and **PDI2**). The introduction of *o*-carborane groups did not alter the optical properties of the PDI units in solution compared to their carborane-free counterparts, maintaining excellent fluorescence quantum yields of around 100% in various solvents. This was achieved by using a methylene linker to minimize electronic interaction between PDI and *o*-carborane, and by incorporating bulky *o*-carborane groups at imide- position to enhance solubility and prevent π–π stacking-induced aggregation. Aggregation studies demonstrated that **PDI–CB1** and **PDI–CB2** have greater solubility than **PDI1** and **PDI2** in both nonpolar and aqueous solvents. Despite the steric hindrance imparted by the *o*-carborane units, the solid state emission of **PDI–CB1** and **PDI–CB2** was affected by aggregation-caused fluorescence quenching. However, solid **PDI–CB1** preserved bright red excimer-type emission, which persisted in water-dispersible nanoparticles, indicating potential for application as a theranostic agent combining fluorescence bioimaging with anticancer boron neutron capture therapy (BNCT) due to its high boron content.

Introduction

During the last years the use of carboranes[1] and metallocarboranes[2] for the preparation of luminescent molecules and materials has raised great attention.[3] As the intrinsic emissive properties of these boron clusters are often poor, the most common strategy explored in the field consists in the conjugation of well-known fluorophores to carborane and metallocarborane units.[3] Different advantages arise from this approach. On the one hand, the resulting systems benefit from the superior chemical and thermal resistance of boron clusters,[1] their high capacity to self-assemble[4] and their improved solubility and cellular uptake.[5] In addition, their rigid 3D geometry can be exploited to control interchromophoric interactions between nearby fluorophores[6] and, as a result, it might lead to aggregation-induced emission (AIE),[3c,7] while preventing aggregation-caused quenching (ACQ).[8] Finally, modulation of the luminescence from the attached emitters can be accomplished both in solution and in the solid state thanks to the particular electronic properties of carboranes and metallacarboranes.[9,10]

However, all these advantages come at the expense of an important limitation: most fluorophore-carborane and fluorophore-metallacarborane conjugates, with a few exceptions,[11] have shown low emission efficiencies in solution due to the quenching effects caused by the boron cluster *via* photoinduced charge transfer (CT).[3,9,10,12] This is clearly illustrated by the case of 1,2-dicarba-*closo*-carborane (*o*-carborane, *o*-CB), which is by far the most used building block for the preparation of these systems. Because of its electron-withdrawing nature, *o*-CB deactivates the emission from nearby electron-rich fluorophores (*e.g.*, anthracene,[9e–g] fluorene[9i,k,l]), which results in low luminescence signals in solution.[3,9] Though this effect can lead to intramolecular CT states displaying intense AIE upon aggregation for sensing and smart material applications,[9] it is a severe restraint if highly emissive *o*-carborane-emitter pairs are to be developed in solution – *e.g.*, for theranostic agents that combine fluorescence diagnosis with anticancer boron neutron capture therapy (BNCT).[12a,b,13]

To overcome this drawback and prevent luminescence quenching in fluorophore-carborane conjugates, two important design principles must be considered: the electronic properties of the emitter and boron cluster, and the nature and length of the linker through which they are attached. Owing to their bright fluorescence and n-type semiconductor character, perylenediimides (PDI)[14] are promising candidates to obtain

[a]*Institut de Ciència de Materials de Barcelona (ICMAB-CSIC), Campus UAB, 08193 Bellaterra, Barcelona, Spain. E-mail: rosario@icmab.es*
[b]*Departament de Química. Universitat Autònoma de Barcelona, E-08193 Bellaterra, Barcelona, Spain. E-mail: jordi.hernando@uab.cat*

†Electronic supplementary information (ESI) available. See DOI: https://doi.org/10.1039/d4dt02477j

‡These authors contributed equally to this work.

highly emissive tethers with *o*-CB in solution, as photoinduced CT between these two units should be disfavored. In addition, the bulkiness of the carborane unit must allow enhancing the solubility of the appended PDIs, which is typically low in most solvents.[14] In spite of these potential advantages, only several examples of PDI–*o*-CB conjugates have so far been described, where the steric effects imparted by the boron cluster were exploited to prevent ACQ and produce luminescent PDI solid materials with relevant sensing, two-photon absorption and electro(fluoro)chromic properties.[6f,8a,b,d,15] However, most of these compounds showed moderate fluorescence efficiencies in solution (Φ_f ~0.1–0.8 [6f,8b,d,15b,c]) that lie clearly below the high emission quantum yields of their constituting PDI dyes (Φ_f ~1 [14]), a detrimental behavior caused by a combination of factors: (a) enhanced intra- and intermolecular PDI–PDI interactions, which are very sensitive to concentration and solvent conditions; and (b) partial intramolecular charge transfer between the PDI and *o*-CB units, which is favored by the use of π-conjugated linkers (*e.g.*, phenyl and phenylacetylene groups) and polar solvents.

Herein we hypothesize that the introduction of carborane clusters as bulky groups in the imide positions of PDIs through a rationally selected linker will prevent intermolecular π–π interactions, thus improving (a) the solubility in organic solvents and (b) the photophysical properties both in solution and solid state to be used as fluorescent dyes. With this aim, compounds **PDI–CB1** and **PDI–CB2** were designed (Scheme 1), which contain: (a) two different, very bright PDI dyes (Φ_f ~0.9–1 [14]), and (b) a non-conjugated methylene linker between the PDI and *o*-CB units, which were tethered through the *N*-imide PDI positions to minimize the effects on the spectral properties of the fluorophore.[14] In the case of **PDI–CB1**, a pristine PDI emitter was used bearing two different lateral *N*-imide substituents: an *o*-CB group and a branched alkyl chain. To further magnify the effect of the boron cluster on solubility, two terminal *o*-CB groups were introduced in **PDI–CB2**, whose 1,6,7,12-tetrachlorinated PDI core is also known to enhance dissolution by minimizing intermolecular π–π interactions.[14] The photophysical properties of these systems have been analyzed in different solvents and in the solid state. Furthermore, nanostructures of the carboranyl-containing PDIs and their properties have also been studied.

Results and discussion

Synthesis of perylenediimide-carborane conjugates

For the synthesis of **PDI–CB1** and **PDI–CB2**, we followed a classical approach for the preparation of *o*-carborane derivatives: the reaction of commercially available decaborane ($B_{10}H_{14}$) with acetylenic compounds to construct the closed structure of the *o*-CB cluster,[16] as previously described for other PDI–*o*-CB conjugates[6f,8a,b,d,15] (Scheme 1). With this aim, we used well-known procedures for the preparation of the *N*-propargylated PDI derivatives **PDI1** [17] and **PDI2** [18] from the commercial perylenetetracarboxylic dianhydride precursor (Scheme S1 in the ESI†).

As shown in Scheme 1a, the insertion reaction of $B_{10}H_{14}$ to the acetylene group of **PDI1** to afford **PDI–CB1** was performed with $AgNO_3$ as a catalyst and acetonitrile as a Lewis base.[19] After optimization of the reaction procedure using different reaction conditions (see Table S1 in ESI†), this led to the target **PDI–CB1** conjugate in 43% yield. By contrast, when the same optimized conditions were employed to produce **PDI–CB2**

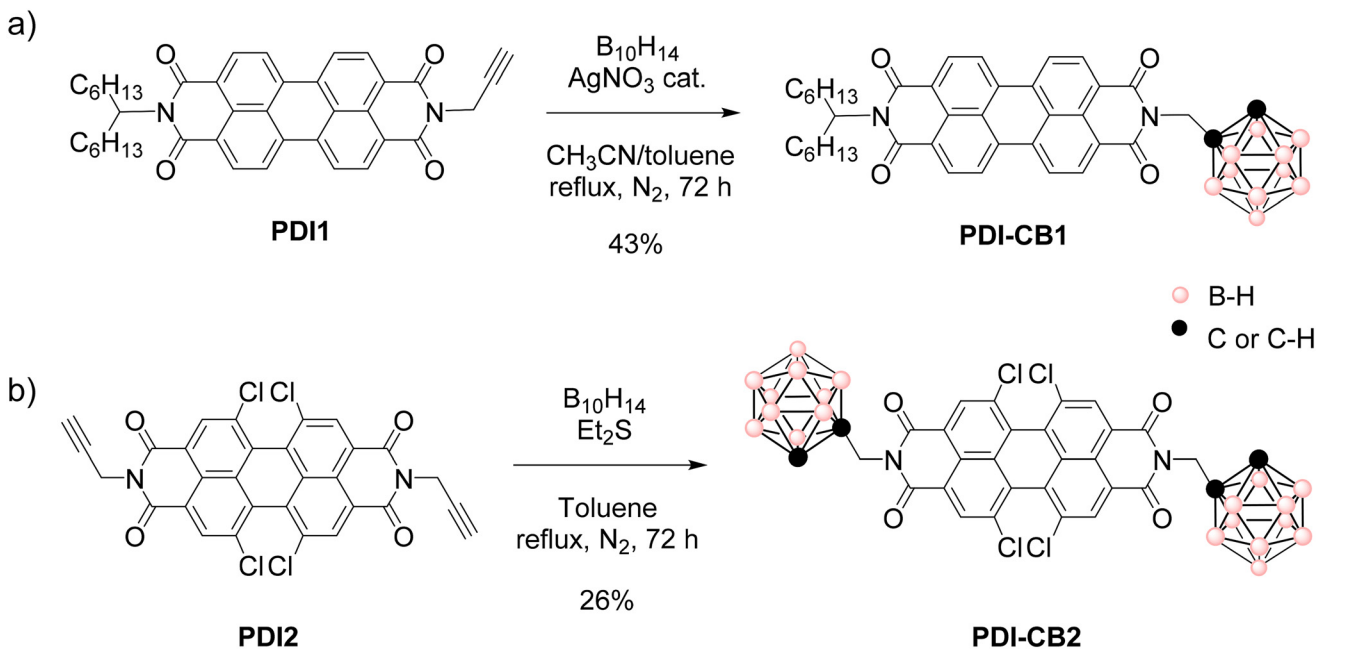

Scheme 1 Insertion reactions to obtain (a) **PDI–CB1** and (b) **PDI–CB2** from $B_{10}H_{14}$ and *N*-propargylated PDIs **PDI1** and **PDI2**.

from **PDI2** and $B_{10}H_{14}$, a very low yield was obtained (15%). For this reason, we applied a different approach for the construction of the *o*-carborane scaffold of **PDI–CB2**,[20] without silver salts, and using SEt_2 as a Lewis base instead of acetonitrile (Scheme 1b). Finally, target compound **PDI–CB2** was obtained with higher yield (26%).

o-Carboranyl derivatives **PDI–CB1** and **PDI–CB2** were characterized by ^{1}H, $^{13}C\{^1H\}$ and $^{11}B\{^1H\}$ NMR, FT-IR spectroscopies and mass spectrometry (MS) (Fig. S7–S14 in the ESI†). In the ^{1}H NMR of **PDI–CB1** and **PDI–CB2**, we observed: (a) the disappearance of the narrow resonance at around 2.25 ppm corresponding to the alkyne proton of precursors **PDI1** and **PDI2**; (b) the appearance of a new resonance at 4.21 ppm and 4.18 ppm for **PDI–CB1** and **PDI–CB2**, respectively, which arise from the $C_{cluster}$–H (C_{CB}–H) of the carborane units introduced in these compounds; and (c) a very broad ^{1}H NMR signal between 3.0–1.0 ppm, which corresponds to the B–H protons of the *o*-CB clusters that cannot be well resolved because of boron-proton coupling. Furthermore, the IR-ATR spectrum of both **PDI–CB1** and **PDI–CB2** showed the broad band characteristic of B–H stretching at around 2580 cm^{-1}, further indicating that the insertion reaction between the PDI precursors and $B_{10}H_{14}$ had occurred. Finally, it must be mentioned that, in the $^{13}C\{^1H\}$ NMR spectrum of **PDI–CB2**, the signals of the C═O group and some of the aromatic carbons were split into two, a feature that has been previously observed for symmetric PDIs bearing very bulky groups at the *N*-imide positions that hinder free rotation of the C–N bond.[21]

Photophysical properties of perylenediimide-carborane conjugates in solution

The UV-Vis absorption and fluorescence properties of the newly designed **PDI–CB1** and **PDI–CB2** were first evaluated in solution. The absorption spectra of these compounds and carboranyl-free perylenediimide dyes **PDI1** and **PDI2** were recorded in acetonitrile at low concentrations ($c < 1.0 \times 10^{-5}$ M, Fig. 1a, Table 1 and Table S2 in the ESI†). All of them showed similar absorption bands, exhibiting several peaks in the visible range of 400–525 nm, which correspond to different vibronic transitions between the ground electronic state (S_0) and the first excited state (S_1) of their PDI core.[14a,b] By contrast, no absorption signals were observed for the *o*-carborane units of **PDI–CB1** and **PDI–CB2**, as they do not absorb at $\lambda_{abs} > 200$ nm.[3] The fact that the absorption spectra of the PDI units in **PDI–CB1** and **PDI–CB2** very much resemble those of the starting, carboranyl-free compounds **PDI1** and **PDI2** can be rationalized on the basis of their electronic structure: the HOMO and LUMO orbitals of PDI chromophores have nodes at the imide nitrogen atoms; as a consequence, derivatization at the *N*-imide positions does not significantly modify their energies.[14a,b] However, changes can occur by functionalization of their *bay* positions due to two main factors:[14a,b] (a) the electronic effects imparted by the substituents introduced on the HOMO and LUMO energies, which can lead to absorption (and emission) spectral shifts; and (b) the steric congestion caused when two non-hydrogen substituents are attached to neighboring *bay* positions, which makes the PDI core take twisted conformations that result in absorption (and emission) broadening with less defined vibronic peaks and lower molar absorptivities. As already reported,[14a,b] the latter is the main factor affecting the absorption of chlorinated PDI derivatives such as **PDI2**, a situation that is also herein reproduced for **PDI–CB2**.

Table 1 Optical properties of **PDI1**, **PDI2**, **PDI–CB1** and **PDI–CB2** in acetonitrile solution

Compound	λ_{abs}^{max} (nm)	ε^a (L mol^{-1} cm^{-1})	λ_f^{max} (nm)	Φ_f
PDI1	520	67 351	530	1.0
PDI–CB1	522	64 295	535	1.0
PDI2	514	35 384	546	0.89
PDI–CB2	519	33 011	552	0.90

[a] Molar absorption coefficients at the spectral maximum.

The emission spectra for all the compounds were also measured in acetonitrile (Fig. 1b, Table 1 and Table S2 in the ESI†). In all the cases, the characteristic PDI emission signals were observed in the range λ_f = 500–700 nm, which correspond to different vibronic bands from the $S_1 \rightarrow S_0$ transition of the

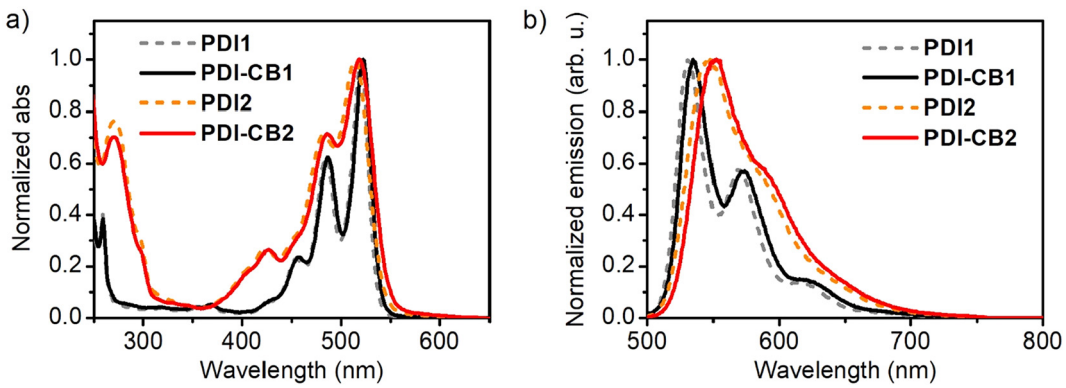

Fig. 1 (a) Absorption ($c = 5.0 \times 10^{-6}$ M) and (b) emission spectra ($c = 2.0 \times 10^{-6}$ M, λ_{exc} = 445 nm) of **PDI–CB1**, **PDI–CB2** and PDI dyes **PDI1** and **PDI2** in acetonitrile. They were all normalized respect to their spectral maximum.

PDI unit.[14a,b] Notably, a ~16 nm bathochromic shift in emission as well as a slight spectral broadening and decrement in Φ_f were measured for **PDI2** and **PDI–CB2** relative to the non-chlorinated dyes **PDI1** and **PDI–CB1**, a series of changes that are normally attributed to the electronic and steric effects imparted by the chlorine substituents introduced.[14a,b] In contrast, very minor differences were observed between the spectra of **PDI–CB1** and **PDI–CB2** and their precursors **PDI1** and **PDI2**. Therefore, the introduction of *o*-carborane clusters at the *N*-imide positions did not alter the emission bands from the nearby PDI fluorophores, except for a small spectral red-shift observed. Very minor changes were also registered for the fluorescent quantum yields of these compounds, as both **PDI–CB1** and **PDI–CB2** preserved the high Φ_f values of the starting PDI dyes **PDI1** and **PDI2** in acetonitrile. Therefore, no electronic interaction takes place between the excited states of the PDI units and the nearby *o*-carborane clusters introduced in the conjugates that could affect their emission efficiency. This is a striking difference with respect to other compounds where *o*-carborane groups are directly attached to other fluorophores different from PDI, where intramolecular charge transfer occurs from the dye (donor unit) to boron clusters (acceptor unit) and leads to significant fluorescence emission quenching (FEQ).[3,9–12] As anticipated above, two main factors should account for this result: (a) the electron-deficient nature of PDIs, which make them poor donors in charge transfer processes; and (b) the introduction of a CH_2 linker between the dye and *o*-carborane units in **PDI–CB1** and **PDI–CB2**.

The high emission efficiency measured for **PDI–CB1** and **PDI–CB2** in acetonitrile also significantly improves the behavior of previously reported carborane-perylenediimide conjugates, which showed moderate Φ_f values (Φ_f ~0.1–0.8 [6f,8b,d,15]), especially when exposed to polar solvents such as acetonitrile. In addition, their superior fluorescent properties were preserved in a wide range of organic media, and a clear decrease in emission quantum yield was only observed for **PDI–CB1** and **PDI–CB2** in a very high polar solvent such as DMSO (Table 2). We ascribe this situation to the particular structure of these compounds. As further discussed below, **PDI–CB1** and **PDI–CB2** exhibit high solubility in a variety of solvents thanks to the presence of the bulky *o*-carborane groups, which disfavors intermolecular PDI–PDI interactions that often detrimentally affect their emission efficiency. Moreover, partial intramolecular charge transfer between the PDI and *o*-carborane units that could lead to fluorescence quenching is disfavored by the use of a methylene linker instead of π-conjugated tethers (*e.g.*, phenyl and phenylacetylene groups).

Table 2 Fluorescence quantum yields of **PDI–CB1** and **PDI–CB2** in different organic solvents

Solvent	PDI–CB1	PDI–CB2
Cyclohexane	0.98	0.91
Dioxane	1.0	0.92
Toluene	1.0	0.92
Chloroform	1.0	0.92
Tetrahydrofuran	1.0	0.91
Dichloromethane	1.0	0.92
Acetonitrile	1.0	0.90
Methanol	0.78	0.89
Dimethylsulfoxide	0.25	0.01

Aggregation studies of PDI–CB1 and PDI–CB2 in solution

As mentioned above, the introduction of bulky carboranyl groups on the *N*-imide positions of PDI fluorophores should enhance their solubility and, therefore, modify their capacity to aggregate in solution. For this reason, we performed aggregation studies for **PDI–CB1**, **PDI–CB2**, **PDI1** and **PDI2** by adding increasing amounts of these compounds in media that are known to be poor solvents for PDI dyes. This should favor molecular aggregation, which in the case of PDI dyes often leads to spectral changes in absorption and emission that can be monitored by UV-vis absorption and fluorescence spectroscopies.[14a]

For the aggregation studies, hexane was first chosen as a solvent because of the poor solubility described for PDI derivatives in this medium.[14a] Actually, *o*-carboranyl-free compounds **PDI1** and **PDI2** showed clear changes in absorption that are consistent with intermolecular aggregation when dissolved in hexane even at relatively low concentrations: new red-shifted absorption bands were registered (λ_{abs}^{max} = 542 nm and 569 nm for **PDI1**, and λ_{abs}^{max} = 555 nm for **PDI2**), while broadening and relative intensity variation of the monomeric PDI absorption bands were also observed (Fig. S1 in the ESI†). This behavior is characteristic of the molecular stacking of PDI cores *via* π–π interactions, which leads to new exciton absorption bands for the aggregates.[14a,22]

Interestingly, when increasing amounts of **PDI–CB1** and **PDI–CB2** were added to hexane, no changes in the absorption spectra were appreciated other than a linear increment of the monomeric absorption intensities (Fig. S2 in the ESI†). This is a clear evidence of the enhancement of their solubility relative to **PDI1** and **PDI2** by the introduction of bulky groups such as carboranes on the *N*-imide positions, which are required to hinder molecular π–π stacking and prevent aggregation.[14a,22] For this reason, we chose dioxane : water mixtures to trigger the molecular aggregation of **PDI–CB1** and **PDI–CB2**, as PDI dyes are normally highly insoluble in aqueous media. Under these conditions, we could register a clear transition from monomer-type to aggregate absorption spectra for increasing concentrations of **PDI–CB1** in 3 : 2 dioxane : water, as proven by the appearance of a red-shifted band and the broadening and relative intensity variation of the monomer signals (Fig. 2a and Fig. S3 in the ESI†). In the case of **PDI–CB2**, less clear spectral changes were observed when monitoring its aggregation in 2 : 3 dioxane : water by UV-vis absorption measurements. In particular, a slight broadening of its absorption spectrum was registered when rising concentration (Fig. 2a and Fig. S3 in the ESI†). The lack of more defined spectral variations upon aggregation for **PDI–CB2** might be due to high molecular disorder and/or large interchromophoric distance in the aggregates, which are known to hinder the occurrence of strong exciton effects.[23] Actually, the latter is expected to

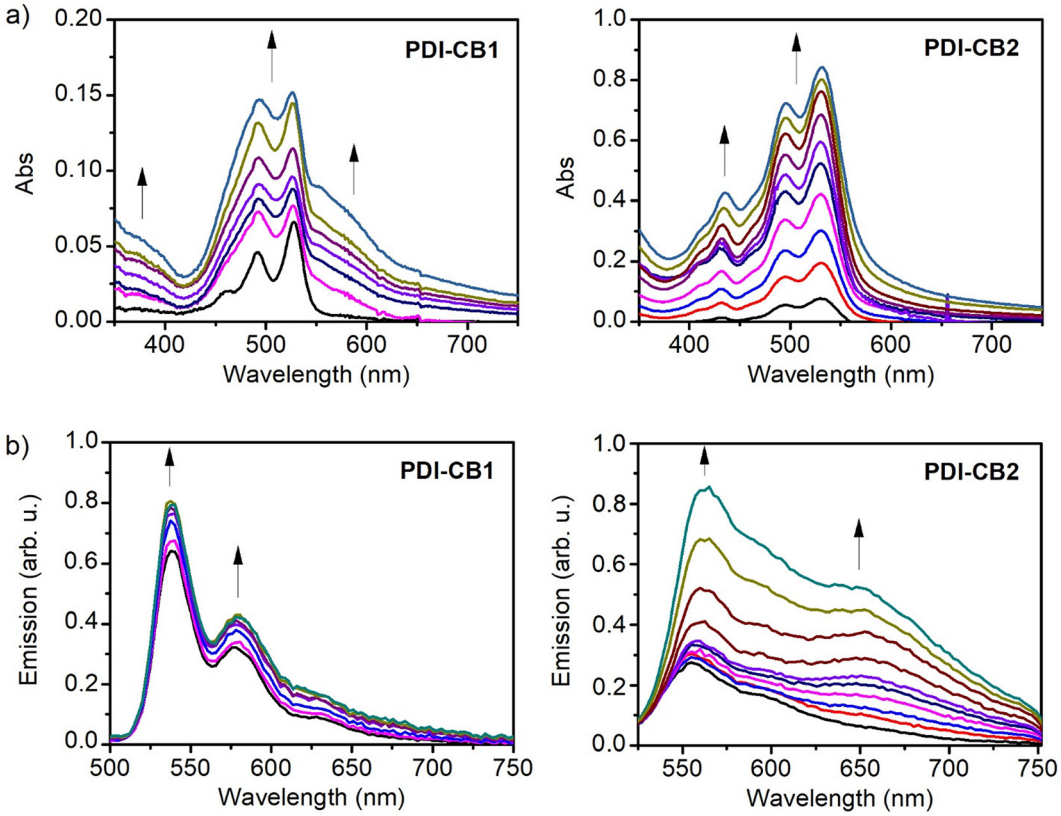

Fig. 2 (a) Variation of the absorption spectrum of **PDI–CB1** and **PDI–CB2** upon consecutive additions of: 5 μL of a stock solution of **PDI–CB1** in dioxane (c = 0.4 × 10^{-3} M) to 2 mL of a 3 : 2 dioxane : water mixture (v = 5, 10, 15, 20, 25, 30 and 35 μL); and 15 μL of a stock solution of **PDI–CB2** in dioxane (c = 0.41 × 0^{-3} M) to 2 mL of a 2 : 3 dioxane : water mixture (v = 15, 30, 45, 60, 75, 90, 105, 120, 135 and 150 μL). (b) Variation of emission spectra (λ_{exc} = 445 nm) of **PDI–CB1** and **PDI–CB2** upon consecutive additions of: 5 μL of a stock solution of **PDI–CB1** in dioxane (c = 0.4 × 10^{-3} M) to 2 mL of a 3 : 2 dioxane : water mixture (v = 5, 10, 15, 20, 25, 30 and 35 μL); and 15 μL of a stock solution of **PDI–CB2** in dioxane (c = 0.41 × 0^{-3} M) to 2 mL of a 2 : 3 dioxane : water mixture (v = 15, 30, 45, 60, 75, 90, 105, 120, 135 and 150 μL). In all the graphs arrows indicate the direction of the spectral changes observed upon consecutive additions of **PDI–CB1** or **PDI–CB2**.

occur for **PDI–CB2** because of the presence of two bulky carboranes side groups as well as the four chlorine *bay* substituents.

Further proof of the aggregation of **PDI–CB1** and **PDI–CB2** in solution was obtained using emission measurements (Fig. 2b). When adding increasing amounts of these compounds to dioxane : water mixtures ($c_{\mathbf{PDI–CB1}}$ = 1.0 × 10^{-6} M–6.9 × 10^{-6} M, $c_{\mathbf{PDI–CB2}}$ = 3.0 × 10^{-6} M–2.8 × 10^{-5} M), low-to-moderate increments of PDI monomer emission at λ_{abs} ~535 (**PDI–CB1**) or 550 nm (**PDI–CB2**) were observed, which indicates that PDI–*o*-CB conjugate molecules efficiently aggregate as their concentration raises. This effect is particularly evident for **PDI–CB1**, as also illustrated by the complementary absorption measurements shown in Fig. 2a. As for the emission of the aggregates formed, it can be correlated with the growth of the new broad and red-shifted band appearing at λ_f > 600 nm, which is of very low intensity for **PDI–CB1** and more clearly visible for **PDI–CB2**. This type of emission is typical for the so-called PDI excimers, which are excited dimers formed in π-stacks of PDI fluorophores that are typically low-emissive.[12a] This feature, together with other interchromophoric interactions expected to take place in the aggregates (*e.g.*, emission quenching by photoinduced electron transfer), explains why the monomer emission bands are still predominant in the spectra shown in Fig. 2b even for high **PDI–CB1** and **PBI–CB2** concentrations where most of these molecules are aggregated. Actually, the formation of dimly red-emitting excimers could be observed by naked eye for larger aggregates of **PDI–CB1** and **PDI–CB2** prepared by simply adding a few droplets of dioxane stock solutions into water (Fig. S4 in the ESI†).

Photophysical properties of perylenediimide-carborane conjugates in the solid state: from bulk powder to nanostructures

In general, PDIs produce vividly colored solutions in organic solvents with intense fluorescence. By contrast, a red-shift of the emission is typically observed in the solid state together with a dramatic decay of the fluorescence efficiency. This is due to the π-stacking of PDI cores, which gives rise to interchromophoric interactions that lead to the formation of excimers, among other types of low- (or non-) emissive species.[14a,22] As a consequence, the optical properties of PDI

derivatives in the solid state are very dependent of molecular packing and there is strong interest to develop compounds of this type that preserve the strong monomeric emission when aggregated, *e.g.*, by introducing bulky groups such as boron clusters that hinder strong interchromophoric interactions at short distances upon aggregation.[6f,8a,b,15b]

To investigate if this behavior is accomplished for **PDI–CB1** and **PDI–CB2**, the diffuse-reflectance absorption and emission spectra of the solid powders of these compounds were measured and compared to those in solution (Fig. 3). In the case of solid **PDI–CB1**, its absorption spectrum resembles those registered for its aggregates in dioxane : water mixtures, as a new red-shifted band and the broadening of the monomer bands were observed (Fig. 3a). This suggests that compact π–π stacking of the PDI units of **PDI–CB1** also takes place in the solid state. As for solid **PDI–CB2**, a similar absorption spectrum to that of the monomer in solution was found. This is the expected behavior according to the aggregation studies performed in solution, as we found tight chromophore packing to be prevented in this case by the steric hindrance imparted by the two *o*-carborane side groups and the chlorine *bay* substituents.

By contrast, the solid powders of **PDI–CB1** and **PDI–CB2** showed a rather similar behavior in emission: the fluorescence bands from monomeric PDI units were not measured and, instead, red excimer-type emission was registered with lower efficiency (Fig. 3b). Therefore, the introduction of *o*-carborane units in the *N*-imide positions of our PDIs could not prevent the formation of excimers due to π–π stacking upon aggregation, thus detrimentally affecting the emissive properties of these fluorophores in the solid state. However, this effect was found to differently impact the fluorescent performance of **PDI–CB1** and **PDI–CB2** powders. On the one hand, the emission of **PDI–CB2** was mainly suppressed in the solid state, as illustrated by the image in the inset of Fig. 3b and corroborated by the Φ_f value measured (Φ_f = 0.012 ± 0.005). In fact, a similar behavior was registered for the solid powder of the reference compound **PDI2** (Φ_f = 0.010 ± 0.006). On the other hand, a much brighter red emission was detected for **PDI–CB1** powder, as demonstrated by the image in the inset of Fig. 3b and the 4-fold higher fluorescence quantum yield measured (Φ_f = 0.045 ± 0.003), which essentially matches the Φ_f value determined for the reference **PDI1** solid sample (Φ_f = 0.045 ± 0.004). As already observed in absorption, the differences between the fluorescent properties of **PDI–CB1** and **PDI–CB2** powders should be attributed to the distinct arrangement of these molecules in the solid state, thus leading to the for-

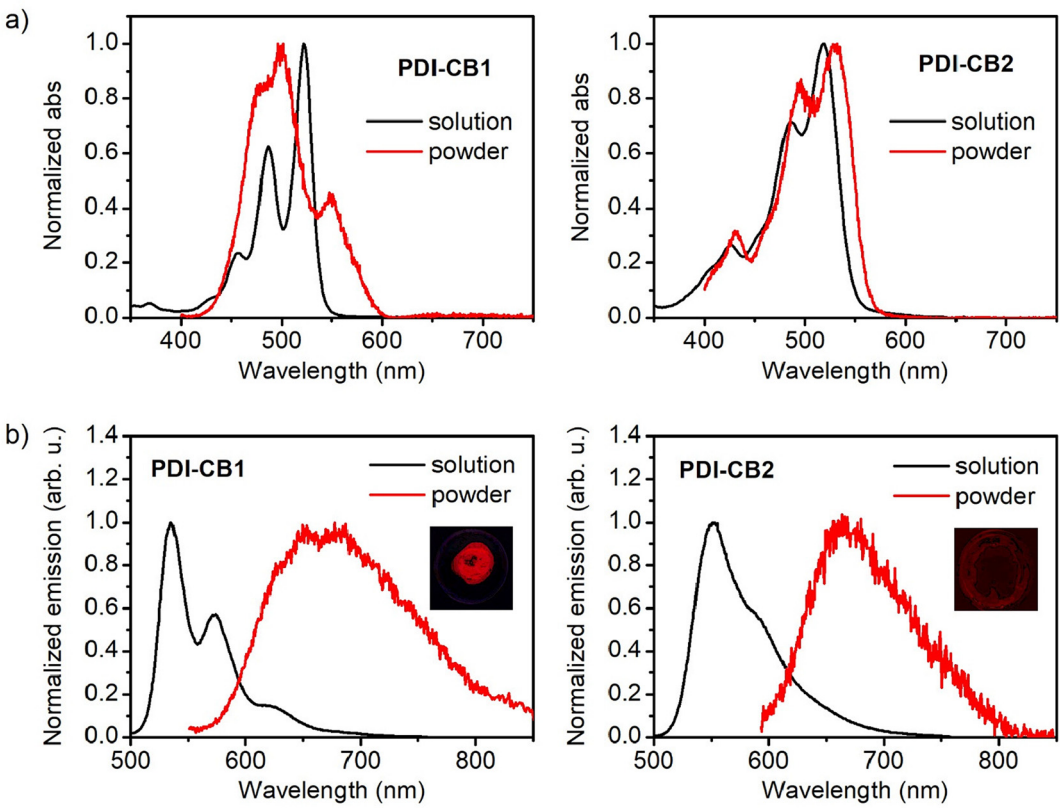

Fig. 3 (a) Absorption spectra of the solid powders obtained from **PDI–CB1** and **PDI–CB2**, which are compared to those measured in acetonitrile solution for both compounds. In the case of powders absorption, the Kubelka–Munk function determined from the diffuse reflectance absorption spectrum is given. For sake of comparison, all the spectra are normalized to unity at their maxima in the visible region. (b) Emission spectra (λ_{exc} = 445 nm) of the solid powders obtained from **PDI–CB1** and **PDI–CB2**, which are compared to those measured in acetonitrile solution for both compounds. The insets in (b) show a photograph of the emission from the powder of each respective compound under irradiation at λ_{exc} = 365 nm.

mation of dissimilar excimer emitting sites and other non-emitting species.

Despite its relatively low fluorescence quantum yield, **PDI–CB1** solid samples exhibit two attractive features for the development of theranostic probes for biological applications: (a) rather bright emission in the red and near-infrared regions (λ_f^{max} ~700 nm) upon irradiation with low-energy visible light (λ_{abs} up to 600 nm, see Fig. 3b), which is often preferred to increase penetration depth and decrease photodegradation and autofluorescence effects in biological tissues; and (b) the high boron content required for efficient boron neutron capture therapy.[24] In light of these properties, we explored the preparation of water-dispersible **PDI–CB1** nanoparticles (**PDI–CB1_NP**). With this aim, we applied the precipitation method[25] followed by purification through dialysis. Transmission electron microscopy (TEM) and dynamic light scattering (DLS) analysis of the resulting nanoparticles revealed that spherical nanostructures of about 100 nm in diameter and good size uniformity were obtained (Fig. 4a, b and Fig. S5, S6 in the ESI†). In addition, the ζ-potential value measured for **PDI–CB1_NP** was around −41.2 mV, thus suggesting good colloidal stability without the need of introducing external stabilizing agents. After storage at 4 °C for two weeks, no changes in TEM and DLS measurements were observed for the NP dispersions.

More importantly, aqueous colloidal suspensions of **PDI–CB_NPs** preserved the principal optical properties of **PDI–CB** bulk powder. Upon visible light excitation, they showed red and near-infrared emission with efficiencies comparable to **PDI–CB1** in the solid state (Φ_f = 0.020, Fig. 4c). In addition, when measuring the fluorescence excitation spectrum of **PDI–CB1_NP** suspensions, the absorption spectrum of **PDI–CB1** bulk powder was reproduced – *i.e.*, a broad absorption spectrum with a red-shifted absorption band extending up to λ_{abs} ~600 nm (Fig. 4c). All these features indicate that excitonic aggregation of the PDI chromophores also occurs in the nanoparticles, where the absorbed excitation energy is funneled towards excimer sites that eventually emit. As a result, **PDI–CB1_NP** generate sufficient red emission under visible light excitation as to be detected by confocal fluorescence microscopy when dispersed onto a glass coverslip (Fig. 4d). This behavior, combined with their high boron content and aqueous dispersibility, would open the door to the use of **PDI–CB1_NP** as theranostic platforms for simultaneous fluorescence detection and boron neutron capture therapy.

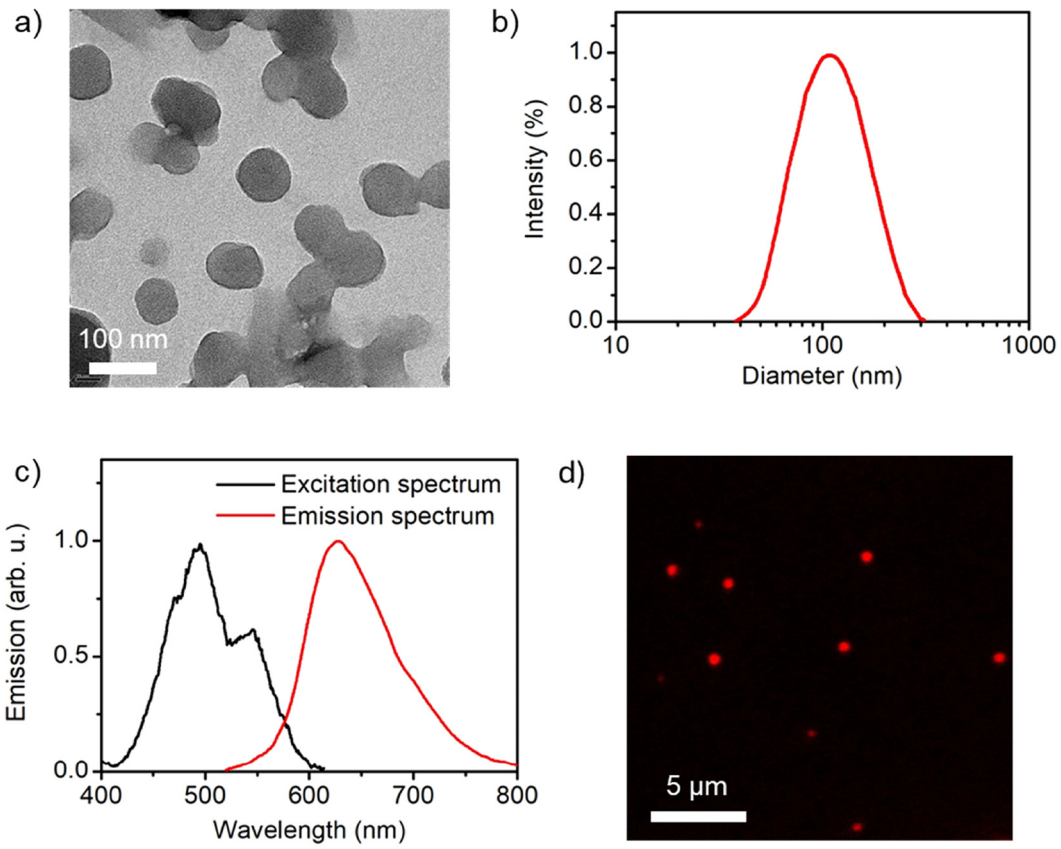

Fig. 4 (a) TEM image of **PDI–CB1_NP** (average diameter = 95 ± 10 nm; see Fig. S6d in the ESI†). (b) Intensity-weighted diameter distributions measured for an aqueous colloidal suspension of **PDI–CB1_NP** by DLS (average diameter = 112 nm; polydispersity index = 0.12). (c) Fluorescence excitation (λ_{em} = 642 nm) and emission (λ_{exc} = 500 nm) spectra of an aqueous colloidal suspension of **PDI–CB1_NP**. (d) Confocal fluorescence microscopy image of **PDI–CB1_NP** casted on a glass coverslip (λ_{exc} = 488 nm, $\lambda_{detection}$ = 520–780 nm).

Conclusions

In this work we have reported the successful synthesis of two perylendiimide (PDI)-based *o*-carborane derivatives (**PDI–CB1** and **PDI–CB2**) *via* the insertion reaction of decaborane with alkyne-terminated PDIs (**PDI1** and **PDI2**). The introduction of *o*-carborane side groups in **PDI–CB1** and **PDI–CB2** did not affect the optical properties of their PDI units in solution relative to their carborane-free counterparts. Remarkably, the synthesized PDI–carborane conjugates retained the high fluorescence quantum yields (Φ_f ~0.9–1) characteristic of PDI fluorophores across a broad range of solvents with varying polarity, which contrasts with most previously reported PDI–*o*-CB derivatives. Two key structural features contributed to this outcome: the use of a methylene linker to minimize through-bond electronic communication between the PDI and carborane units, and the enhanced solubility provided by the bulky carborane groups positioned at the *N*-imide sites of the PDI chromophores, thereby preventing aggregation *via* π–π stacking. Aggregation studies confirmed that **PDI–CB1** and **PDI–CB2** exhibited significantly higher solubility than their parent PDI compounds, **PDI1** and **PDI2**, in both nonpolar organic solvents (*e.g.*, hexane) and aqueous environments (*e.g.*, dioxane mixtures). Nevertheless, despite the steric hindrance introduced by the *o*-carborane substituents, fluorescence quenching due to aggregation was observed for **PDI–CB1** and **PDI–CB2** in the solid state. Yet, **PDI–CB1** preserved rather bright red excimer-type emission in its solid form, which was maintained upon formation of water-dispersible nanoparticles that could be detected by confocal fluorescence microscopy. Given their low-energy emission characteristics and high boron content, these nanostructures may have potential applications as theranostic agents for bioimaging and BNCT. In light of the promising results obtained in this work, the development of novel PDI–CB conjugates holds potential. These new conjugates could exhibit enhanced emission efficiencies in the solid state, coupled with valuable optoelectronic properties.

Experimental section

Materials

Commercial reagents were used as received from suppliers. The anhydrous MeOH was kept over molecular sieves 3 Å. Decaborane ($B_{10}H_{14}$) was purchased by Katchem Ltd (Prague) and recrystallized before use. Toluene was purchased from Merck and distilled from sodium benzophenone previously to use. 7-Tridecanone, perylene-3,4,9,10-tetracarboxylic dianhydride, ammonium acetate, sodium cyanoborohydride, NaOH, KOH, imidazole, K_2CO_3, Et_3N, $AgNO_3$ and Et_2S were purchased from Sigma-Aldrich and utilized as received. HPLC grade hexane, dioxane, $CHCl_3$, MeOH, CH_2Cl_2, acetonitrile and DMSO were obtained from Scharlab and used without further purification.

All reactions were performed under inert atmosphere employing standard Schlenk techniques. Thin layer chromatography (TLC) was performed on pre-coated aluminum layers of silica gel 60 F254 (0.20 mm thick): MACHEREY-NAGEL Alugram® silica plates SIL G/UV_{254}. Preparative TLC was performed on Pre-coated TLC-plates SIL HD; 0.25 mm thick silica gel 60. Flash column chromatography was performed by using silica gel (SiO_2) with 0.04–0.06 mm in particle size and 60 Å in pore size.

Instruments

Infrared spectra were recorded using a Bruker Tensor 27 spectrometer equipped with a Golden Gate Single Reflection Diamond ATR. Nuclear magnetic resonance (NMR) spectra were recorded with Bruker DPX-250 and DPX-360 (^{1}H NMR (250 MHz, 360 MHz, 400 MHz), and DPX-400 spectrometers (^{11}B and ^{11}B{^{1}H} NMR (128 MHz)) and ^{13}C{^{1}H} NMR (100, MHz)). Chemical shifts are reported in ppm using the signal of the residual non-deuterated solvent molecules as a reference for ^{1}H NMR and ^{13}C{^{1}H} NMR. For ^{11}B and ^{11}B{^{1}H} NMR, spectra were measured using quartz tubes and referenced to external $BF_3{\cdot}OEt_2$. All coupling constants are reported in hertz. MALDI-TOF-MS mass spectra were recorded in the negative ion mode using a Bruker Biflex MALDI-TOF spectrometer and dithranol (DIT) as a matrix.

UV-vis absorption spectra in solution were recorded in a HP 8452A spectrophotometer (Agilent) with Chemstation software, using 0.1- or 1 cm optical path quartz cuvettes and HPLC-quality solvents. For solid samples, an Agilent Cary 60 spectrophotometer in diffuse reflectance mode and coupled to a remote integrating sphere was used. In this case, the Kubelka–Munk function was used to estimate their absorption spectra. Fluorescence emission spectra were measured in a custom-made spectrofluorometer by using CW laser excitation at λ_{exc} = 445 nm and detecting the emitted photons in an Andor ICCD camera coupled to an Andor spectrograph. All the emission spectra registered were corrected by the wavelength dependence of the spectral response of the detection system. Samples were prepared in HPLC grade solvents and adjusted to a response within the linear range. Fluorescence quantum yields in solution were determined using the standard method[26] for highly diluted solutions of the compounds of interest to prevent self-absorption processes (absorption <0.1 at the excitation wavelength) and relative to *N*,*N*′-bis(1-hexylheptyl)perylene-3,4,9,10-tetracarboxybismide in acetonitrile (Φ_f = 1).[27] For solid samples, absolute fluorescence quantum yields were determined using a Hamamatsu Quantum Yield fluorometer C9920-02G using an integrating sphere.

Scanning electron microscopy images of the nanostructures were obtained in a MERLIN FE-SEM microscope. Dynamic light scattering (DLS) measurements to characterize the nanoparticle diameters and ζ-potentials were measured in a Malvern Zetasizer Nano ZS apparatus. Confocal fluorescence microscopy images were acquired in a Leica TCS SP5 microscope using an air objective (20×, NA = 0.70) and an Ar laser (λ = 488 nm) as excitation source.

Synthetic procedures

The synthesis of the already reported precursors **PDI1** and **PDI2** is provided in the ESI.†

PDI–CB1. Decaborane ($B_{10}H_{14}$) (44 mg, 0.36 mmol) was dissolved in CH_3CN (8.0 mL, 152 mmol) and heated under reflux

for 2 h. Then, diimide **PDI1** (63.0 mg, 0.12 mmol) dissolved in 12 mL of anhydrous toluene in the presence of $AgNO_3$ (8.3 mg, 0.05 mmol) was added to the $B_{10}H_{12}{\cdot}(CH_3CN)_2$ adduct mixture with a syringe and heated under reflux for 72 h under nitrogen atmosphere. The reaction mixture was cooled down to room temperature, diluted with 15 mL of toluene and filtered through Celite. The resulting orange fluorescent solution was concentrated under reduced pressure and purified by flash column chromatography ($CHCl_3$) to obtain pure **PDI–CB1** (32.0 mg, 43% yield) as a red solid. **^{1}H NMR** (250 MHz, $CDCl_3$, δ): 8.82–8.43 (m, 8H), 5.18 (m, 1H), 4.96 (s, 2H), 4.21 (s, C_{CB}–H), 2.36–2.09 (m, 2H), 1.98–1.73 (m, 2H), 1.47–1.04 (m, 16H), 0.85 (t, J = 9.1 Hz, 6H) ppm. Because of ^{11}B quadrupole moment, B–H nuclei do not give rise to clear peaks in the ^{1}H NMR spectrum but a broad signal from 3.00–1.00 ppm. **^{13}C {^{1}H} NMR** (100 MHz, $CDCl_3$, δ): 163.1, 135.7, 133.8, 132.3, 129.6, 129.4, 126.5, 126.2, 123.6, 123.0, 121.7, 73.5, 61.1, 55.0, 44.3, 31.8, 29.2, 27.0, 22.6, 14.0, 1.0 ppm. **^{11}B{^{1}H} NMR** (128 MHz, $CDCl_3$, δ): −1.18 (s, 2B), −4.59 (s, 2B), −10.11 (s, 4B), −12.17 (s, 2B) ppm. **IR** (ATR, ν): 3085, 2924, 2855, 2583 (B–H), 1698 (C═O imide), 1652 (C═O imide), 1593, 1578, 1436, 1403, 1337, 1250, 1177, 1108, 1066, 1017, 852, 809, 746, 725, 675, 645 cm^{-1}. **MS** (MALDI, m/z): calculated for $[C_{40}H_{47}B_{10}N_2O_4]^+$: 729.5; found 729.9 (M − H).

PDI–CB2. Et_2S (0.2 mL, 1.86 mmol) was added to a 2.2 mL of anhydrous toluene solution of $B_{10}H_{14}$ (116.0 mg, 0.95 mmol) and the mixture was stirred at room temperature for 30 min. Then, diimide **PDI2** (101.0 mg, 0.17 mmol) was dissolved in 8.6 mL of anhydrous toluene and was added to the decaborane solution mixture with a syringe. The resulting mixture was heated under reflux for 72 h under nitrogen atmosphere. Afterwards, it was cooled down to room temperature and the solvent was removed under vacuum. The resulting black solid was dissolved in 25 mL of MeOH, filtered and washed with toluene. The resulting orange-greenish fluorescent filtered solution was concentrated under reduced pressure and purified by flash column chromatography ($CHCl_3$) to obtain pure **PDI–CB2** (37.1 mg, 26% yield) as a red solid. **^{1}H NMR** (250 MHz, $CDCl_3$, δ): 8.73 (m, 4H), 4.96 (s, 4H), 4.18 (s, 2H, C_{CB}–H) ppm. Because of ^{11}B quadrupole moment, B–H nuclei do not give rise to clear peaks in the ^{1}H NMR spectrum but a broad signal from 3.00–1.00 ppm. **^{13}C NMR** (100 MHz, $CDCl_3$, δ) 162.1, 162.0, 136.0, 135.9, 135.9, 135.8, 133.9, 133.9, 133.8, 133.8, 131.5, 129.3, 129.2, 123.3, 122.2, 122.2, 73.0, 61.2, 44.5, 29.3 ppm. **^{11}B{^{1}H} NMR** (128 MHz, $CDCl_3$, δ) −1.17 (s, 4B), −4.46 (s, 4B), −9.83 (br s, 6B), −12.66 (br s, 6B) ppm. **IR** (ATR, ν) 3068, 2923, 2853, 2577 (B–H), 1708, 1668, 1587, 1420, 1390 1360, 1288, 1239, 1185, 1115, 1077, 1017, 904, 871, 824, 802, 749, 726, 686 cm^{-1}. **MS** (MALDI, m/z): calculated for $[C_{30}H_{30}B_{20}Cl_4N_2O_4]^+$: 842.3; found 842.3.

Author contributions

R. R. – performed the synthesis of the compounds, the characterization of their optical properties and data analysis; S. S. – performed nanostructure preparation and characterization; L. P. – contributed to the synthetic and optical characterization work; J. H. – performed data analysis, supervised the project, prepared the original draft and acquired funding; R. N. – supervised the project, prepared the original draft and acquired funding. All authors have read and approved the final version.

Data availability

The authors declare that all data underlying the results are available as part of the main article and the data supporting this article have been included as part of the ESI.† No additional source data are required.

Conflicts of interest

There are no conflicts to declare.

Acknowledgements

This work was supported by grants PID2022-141293OB-I00 and PID2022-136892NB-I00 funded by MICIU/AEI/10.13039/501100011033 and by ERDF – "A way of making Europe". R. Núñez acknowledges financial support from the State Investigation Agency, through the Severo Ochoa Programme for Centers of Excellence in R&D (CEX2023-001263-S). Financial support from the Generalitat de Catalunya (AGAUR) is also acknowledged through 2021 SGR 00064 and 2021 SGR 00442 projects. S. S. acknowledges financial support from DOC-FAM, the European Union's Horizon 2020 research and innovation program under the Marie Sklodowska-Curie grant agreement no 754397. L. P. thanks to the Universitat Autònoma de Barcelona for her predoctoral fellowship. J. H. is a Serra Húnter Fellow.

References

1 (*a*) R. N. Grimes, *Carboranes*, Academic Press, Amsterdam, 3rd edn, 2016; (*b*) M. Scholz and E. Hey-Hawkins, *Chem. Rev.*, 2011, **111**, 7035–7062; (*c*) C. Viñas, *Future Med. Chem.*, 2013, **5**, 617–619.

2 (*a*) C. E. Housecroft, *Boron: Metallacarbaboranes, Encyclopedia of Inorganic and Bioinorganic Chemistry*, Wiley, 2011; (*b*) P. Farràs, E. J. Juárez-Pérez, M. Lepsik, R. Luque, R. Núñez and F. Teixidor, *Chem. Soc. Rev.*, 2012, **41**, 3445–3463.

3 (*a*) R. Núñez, M. Tarrès, A. Ferrer-Ugalde, F. F. de Biani and F. Teixidor, *Chem. Rev.*, 2016, **116**, 14307–14378; (*b*) S. Mukherjee and P. Thilagar, *Chem. Commun.*, 2016, **52**, 1070–1093; (*c*) J. Ochi, K. Tanaka and Y. Chujo, *Angew. Chem., Int. Ed.*, 2020, **59**, 9841–9855; (*d*) A. Marfavi,

P. Kavianpour and L. M. Rendina, *Nat. Rev. Chem.*, 2022, **6**, 486–504.

4 (*a*) J. N. Hohman, P. Zhang, E. I. Morin, P. Han, M. Kim, A. R. Kurland, P. D. McClanahan, V. P. Balema and P. S. Weiss, *ACS Nano*, 2009, **3**, 527–536; (*b*) D. Brusselle, P. Bauduin, L. Girard, A. Zaulet, C. Viñas, F. Teixidor, I. Ly and O. Diat, *Angew. Chem., Int. Ed.*, 2013, **52**, 12114–12118.

5 (*a*) C. Viñas and E. Hey-Hawkins, *Boron-Based Compounds: Potential and Emerging Applications in Medicine*, Wiley, 2018; (*b*) F. Issa, M. Kassiou and L. M. Rendina, *Chem. Rev.*, 2011, **111**, 5701–5722; (*c*) C. Viñas, R. Núñez, I. Bennour and F. Teixidor, *Curr. Med. Chem.*, 2019, **26**, 5036–5076.

6 (*a*) R. Ziessel, G. Ulrich, J. H. Olivier, T. Bura and A. Sutter, *Chem. Commun.*, 2010, **46**, 7978–7980; (*b*) A. Harriman, M. A. H. Alamiry, J. P. Hagon, D. Hablot and R. Ziessel, *Angew. Chem., Int. Ed.*, 2013, **52**, 6611–6615; (*c*) D. Hablot, R. Ziessel, M. A. H. Alamiry, E. Bahraidah and A. Harriman, *Chem. Sci.*, 2013, **4**, 444–453; (*d*) A. V. Safronov, N. I. Shlyakhtina, T. A. Everett, M. R. VanGordon, Y. V. Sevryugina, S. S. Jalisatgi and M. F. Hawthorne, *Inorg. Chem.*, 2014, **53**, 10045–10053; (*e*) X. Wu, J. Guo, J. Zhao, Y. Che, D. Jia and Y. Chen, *Dyes Pigm.*, 2018, **154**, 44–51; (*f*) C. Sang, G. Wang, Y.-C. Wei, Q. Jiang, K. Liu, M. Zhang, Y.-Y. Chen, X. Chang, F. Liu, S. Yin, P.-T. Chou and Y. Fang, *CCS Chem.*, 2022, **4**, 1949–1960.

7 (*a*) K. Kokado and Y. Chujo, *Macromolecules*, 2009, **42**, 1418–1420; (*b*) J. Cabrera-González, C. Viñas, M. Haukka, S. Bhattacharyya, J. Gierschner and R. Núñez, *Chem. – Eur. J.*, 2016, **22**, 13588–13598; (*c*) M. Chaari, Z. Kelemen, J. G. Planas, F. Teixidor, D. Choquesillo-Lazarte, A. Ben Salah, C. Viñas and R. Núñez, *J. Mater. Chem. C*, 2018, **6**, 11336–11347; (*d*) Y. Yin, X. Li, S. Yan, H. Yan and C. Lu, *Chem. – Asian J.*, 2018, **13**, 3155–3159; (*e*) X. Wei, M.-J. Zhu, Z. Cheng, M. Lee, H. Yan, C. Lu and J. J. Xu, *Angew. Chem., Int. Ed.*, 2019, **58**, 3162–3166.

8 (*a*) K. Liu, C. Shang, Z. Wang, Y. Qi, R. Miao, K. Liu, T. Liu and Y. Fang, *Nat. Commun.*, 2018, **9**, 1695; (*b*) K. Liu, Z. Wang, C. Shang, X. Li, H. Peng, R. Miao, L. Ding, J. Liu, T. Liu and Y. Fang, *Adv. Mater. Technol.*, 2019, **4**, 1800644; (*c*) N. Ding, K. Liu, Y. Qi, C. Shang, X. Chang and Y. Fang, *Sens. Actuators, B*, 2021, **340**, 129964; (*d*) Z. Wang, X. Gou, S. K. Liu, X. Chang, G. Wang, W. Xu, S. Lin, T. Liu and Y. Fang, *Angew. Chem., Int. Ed.*, 2022, **61**, e202207619.

9 (*a*) K. Kokado and Y. Chujo, *J. Org. Chem.*, 2011, **76**, 316–319; (*b*) L. Weber, J. Kahlert, R. Brockhinke, L. Böhling, A. Brockhinke, H.-G. Stammler, B. Neumann, R. A. Harder and M. A. Fox, *Chem. – Eur. J.*, 2012, **18**, 8347–8357; (*c*) K. Nishino, H. Yamamoto, K. Tanaka and Y. Chujo, *Org. Lett.*, 2016, **18**, 4064–4067; (*d*) R. Furue, T. Nishimoto, I. S. Park, J. Lee and T. Yasuda, *Angew. Chem., Int. Ed.*, 2016, **55**, 7171–7175; (*e*) D. Tu, P. Leong, Z. Li, R. Hu, C. Shi, K. Y. Zhang, H. Yan and Q. A. Zhao, *Chem. Commun.*, 2016, **52**, 12494–12497; (*f*) H. Naito, K. Nishino, Y. Morisaki, K. Tanaka and Y. Chujo, *J. Mater. Chem. C*, 2017, **5**, 10047–10054; (*g*) X. Wu, J. Guo, Y. Quan, W. Jia, D. Jia, Y. Chen and Z. Xie, *J. Mater. Chem. C*, 2018, **6**, 4140–4149; (*h*) N. V. Nghia, S. Jana, S. Sujith, J. Y. Ryu, J. Lee, S. U. Lee and M. H. Lee, *Angew. Chem., Int. Ed.*, 2018, **57**, 12483–12488; (*i*) K. L. Martin, J. N. Smith, E. R. Young and K. R. Carter, *Macromolecules*, 2019, **52**, 7951–7960; (*j*) Y.-J. Cho, S.-Y. Kim, J.-W. Lee, W.-S. Han, C. H. Kim, H.-J. Son and S. O. Kang, *Chem. – Eur. J.*, 2019, **25**, 8149–8156; (*k*) M. S. Mun, C. H. Ryu, H. So, M. Kim, J. H. Lee, H. Hwang and K. M. Lee, *J. Mater. Chem. C*, 2020, **8**, 16896–16906; (*l*) S. Sinha, Z. Kelemen, E. Hümpfer, I. Ratera, J.-P. Malval, J. P. Jurado, C. Viñas, F. Teixidor and R. Núñez, *Chem. Commun.*, 2022, **58**, 4016–4019; (*m*) H. Yang, H. Liu, Y. Shen, S.-T. Zhang, Q. Zhang, Q. Song, C. Lv, C. Zhang, B. Yang, Y. Ma and Y. Zhang, *Angew. Chem.*, 2022, **134**, e202115551.

10 (*a*) K. C. Song, H. Kim, K. M. Lee, Y. S. Lee, Y. Do and M. H. Lee, *Dalton Trans.*, 2013, **42**, 2351–2354; (*b*) N. V. Nghia, J. Oh, S. Sujith, J. Jung and M. H. Lee, *Dalton Trans.*, 2018, **47**, 17441–17449; (*c*) L. Parejo, M. Chaari, S. Santiago, G. Guirado, F. Teixidor, R. Núñez and J. Hernando, *Chem. – Eur. J.*, 2021, **27**, 270–280.

11 D. Tu, P. Leong, Z. Li, R. Hu, C. Shi, K. Y. Zhang, H. Yan and Q. Zhao, *Chem. Commun.*, 2016, **52**, 12494–12497.

12 (*a*) M. Chaari, N. Gaztelumendi, J. Cabrera-González, P. Peixoto-Moledo, C. Viñas, E. Xochitiotzi-Flores, N. Farfán, A. Ben Salah, C. Nogués and R. Núñez, *Bioconjugate Chem.*, 2018, **29**, 1763–1773; (*b*) J. Cabrera-González, B. M. Muñoz-Flores, C. Viñas, A. Chávez-Reyes, H. V. R. Dias, V. M. Jiménez-Pérez and R. Núñez, *Chem. – Eur. J.*, 2018, **24**, 5601–5612; (*c*) C. Bellomo, M. Chaari, J. Cabrera-González, M. Blangetti, C. Lombardi, A. Deagostino, C. Viñas, N. Gaztelumendi, C. Nogués, R. Núñez and C. Prandi, *Chem. – Eur. J.*, 2018, **24**, 15622–15630.

13 W. Ma, Y. Wang, Y. Xue, M. Wang, C. Lu, W. Guo, Y.-H. Liu, D. Shu, G. Shao, Q. Xu, D. Tu and H. Yan, *Chem. Sci.*, 2024, **15**, 4019–4030.

14 (*a*) F. Würthner, *Chem. Commun.*, 2004, 1564–1579; (*b*) F. Würthner, C. R. Saha-Möller, B. Fimmel, S. Ogi, P. Leowanawat and D. Schmidt, *Chem. Rev.*, 2015, **116**, 962–1052; (*c*) A. Nowak-Król and F. Würthner, *Org. Chem. Front.*, 2019, **6**, 1272–1318.

15 (*a*) C. Hua, K. Liu, Y. Wu, W. Xu, J. Zhang, Z. Wang, K. Liu and Y. Fang, *ACS Appl. Mater. Interfaces*, 2021, **13**, 49500–49508; (*b*) W. Feng, K. Liu, J. Zang, J. Xu, H. Peng, L. Ding, T. Liu and Y. Fang, *J. Phys. Chem. B*, 2021, **125**, 11540–11547; (*c*) W. Feng, Q. Jiang, Z. Wang, J. Zang, G. Wang, K. Liu, H. Peng, T. Liu, L. Ding and Y. Fang, *J. Phys. Chem. B*, 2022, **126**, 4939–4947.

16 (*a*) T. L. Heying, J. W. Ager, S. L. Clark, D. J. Mangold, H. L. Goldstein, M. Hillman, R. J. Polak and J. W. Szymanski, *Inorg. Chem.*, 1963, **2**, 1089–1092; (*b*) M. Thornton-Pett, M. A. Beckett and J. D. Kennedy, *J. Chem. Soc., Dalton Trans.*, 1986, 303–308.

17 (*a*) H. Langhals and A. Obermeier, *Eur. J. Org. Chem.*, 2008, 6144–6151; (*b*) D. Shanks, S. Preus, K. Qvortrup, T. Hassenkam, M. B. Nielsen and K. Kilså, *New J. Chem.*, 2009, **33**, 507–516.

18 (*a*) K.-R. Wang, H.-W. An, F. Qian, Y.-Q. Wang, J.-C. Zhang and X.-L. Li, *RSC Adv.*, 2013, **3**, 23190–23196; (*b*) K. Sun, C. Xiao, C. Liu, W. Fu, Z. Wang and Z. Li, *Langmuir*, 2014, **30**, 11040–11045.
19 A. Toppino, A. R. Genady, M. E. El-Zaria, J. Reeve, F. Mostofian, J. Kent and J. F. Valliant, *Inorg. Chem.*, 2013, **52**, 8743–8749.
20 N. Shin, S. Yu, J. H. Lee, H. Hwang and K. M. Lee, *Organometallics*, 2017, **36**, 1522–1529.
21 L. D. Wescott and D. L. Mattern, *J. Org. Chem.*, 2003, **68**, 10058–10066.
22 K. Balakrishnan, A. Datar, T. Naddo, J. Huang, R. Oitker, M. Yen, J. Zhao and L. Zang, *J. Am. Chem. Soc.*, 2006, **128**, 7390–7398.
23 M. Kasha, H. R. Rawls and M. A. El-Bayoumi, *Pure Appl. Chem.*, 1965, **11**, 371–392.
24 (*a*) C. Viñas and E. Hey-Hawkins, *Boron-Based Compounds: Potential and Emerging Applications in Medicine*, Wiley, 2018; (*b*) C. Viñas, R. Núñez, I. Bennour and F. Teixidor, *Curr. Med. Chem.*, 2019, **26**, 5036–5076.
25 S. Sinha, Z. Kelemen, E. Hümpfner, I. Ratera, J. P. Marval, J. P. Jurado, C. Viñas, F. Teixidor and R. Núñez, *Chem. Commun.*, 2022, **58**, 4016–4019.
26 J. R. Lakowicz, Principles of Fluorescence Spectroscopy, Springer, New York, 2006.
27 T. Kircher and H.-G. Löhmannsröben, *Phys. Chem. Chem. Phys.*, 1999, **1**, 3987–3992.